physica status solidi b
www.pss-b.com

# Nanoindentation Creep Behavior of Single-Crystal $Bi_2Se_3$ Topological Insulator

*Utku Uzun,* Caterina Lamuta, and Mehmet Yetmez*

**A single-crystal $Bi_2Se_3$ topological insulator is fabricated using the Bridgman–Stockbarger method. The crystal structure and atomic lattice parameters are identified by X-ray diffraction analysis. The nanoindentation size effect on creep displacement, activation volume, and strain rate sensitivity (SRS) with different maximum holding loads between 1000 and 5000 μN is investigated using depth-sensing nanoindentation. Furthermore, the effect of the loading rate on the steady-state creep displacement and SRS is analyzed and discussed. Results show $Bi_2Se_3$'s low resistance to plastic deformation and a significant increase of creep displacement with increasing holding load and holding rate. Additionally, creep strain rate, activation volume, and SRS are also calculated from the secondary stage creep, and results are compared with those of other flexible electronic materials.**

## 1. Introduction

Topological insulators (TIs) are a novel class of advanced materials that behave as electrical insulators in the bulk and can conduct electricity on their surfaces or edges.[1,2] TIs can hold Majorana fermions (i.e., particles that act as their own antiparticles and can be used as qubits or individual computational parts). A qubit is thought to be made up of combinations of Majorana fermion pairs, each of which will be separated from its partner. If one member of the couple is affected by noise-induced errors, the other remains unaffected. In other words, it should preserve the integrity of the qubit and ensure that it performs a calculation correctly in a way that is least affected by these errors.[3,4] This unique property has made TIs the number one candidate for high-tech applications, such as spintronics[5] and quantum computers.[6]

U. Uzun
Department of Aerospace Engineering
Tarsus University
Tarsus/Mersin 33400, Turkey
E-mail: utkuuzun@tarsus.edu.tr

U. Uzun, C. Lamuta
Department of Mechanical Engineering
University of Iowa
Iowa City, IA 52242, USA

M. Yetmez
Department of Mechanical Engineering
Zonguldak Bülent Ecevit University
Zonguldak 67100, Turkey

The ORCID identification number(s) for the author(s) of this article can be found under https://doi.org/10.1002/pssb.202100481.

**DOI: 10.1002/pssb.202100481**

Bismuth chalcogenides such as bismuth telluride ($Bi_2Te_3$)[7] and bismuth selenide ($Bi_2Se_3$)[8] have been recently identified as promising TIs due to their topologically protected surface states. However, due to the high cost and toxicity of tellurium,[9] $Bi_2Se_3$ represents a more versatile TI, and has been the focus of several scientific studies in the past decade. Although several works have been proposed to study the physical and electrical properties of $Bi_2Se_3$,[10,11] studies on the mechanical properties of $Bi_2Se_3$ remain limited. Lai et al.[12] measured the hardness and Young's modulus of $Bi_2Se_3$ thin films and discussed the interplay between plastic deformation and pop-in behavior. Gupta et al.[13] investigated both the thermal and the mechanical behavior of single-crystal $Bi_2Se_3$ and concluded that high-quality single crystals present lower hardness and Young's modulus values than polycrystalline samples. Their results were confirmed by Yan et al.,[14] who observed that relatively large crystal defects can have a detrimental effect on the mechanical properties of $Bi_2Se_3$.

No literature works have been proposed to study the time-dependent mechanical behavior of the bulk single-crystal $Bi_2Se_3$, which represents crucial information for the design of $Bi_2Se_3$-based devices, such as field-effect transistors,[15] solar cells,[16] and metaphotonics.[17] The time-dependent deformation of materials under constant stress, known as creep, provides information on the material's behavior under long-term static loads[18] and allows the designer to predict the redistribution of internal forces that can lead to potential failure.[19]

In this study, the creep behavior of a 3D bulk single-crystal $Bi_2Se_3$ TI, grown by the Bridgman–Stockbarger method, is investigated for the first time by using depth-sensing indentation (DSI). Contrary to conventional creep tests performed using conventional uniaxial tensile testing machines which are only suitable for macro-scale samples, DSI is able to measure the mechanical properties of thin films and small samples at the nano-scale and micro-scale by monitoring the penetration depth and the applied load of a diamond tip that penetrates the material's surface.[20] The small-scale and localized nature of DSI measurements, not affected by the influence of macro-scale defects, represents a great advantage for the study of single crystals' properties.[21]

A wide range of loading rates (between 55.55 and 1000 $\mu N\ s^{-1}$) was applied to study the creep behavior of $Bi_2Se_3$ at room temperature, and different time-dependent properties such as

 

creep displacement, activation volume, and strain rate sensitivity (SRS) were measured and compared with those other flexible electronic materials.

## 2. Experimental Section

$Bi_2Se_3$ single-crystal samples were grown using the Bridgman–Stockbarger method.[22] The starting polycrystalline sample, synthesized from high-purity (99.999%) elements, was placed in a quartz ampoule with a conical base and sealed under vacuum ($10^{-5}$ Pa). The ampoule was held in the hot zone for 12 h to achieve homogenization and then moved from the hot zone (1050 K) to the cold zone (900 K) with a speed of 1.0 mm $h^{-1}$ (suggested value to obtain good quality crystals[23]). The final sample, which presented a half-pyramidal shape, was fixed alongside its cleavage plane to obtain a (0001) oriented surface.[24] The crystal structure of the grown $Bi_2Se_3$ sample was analyzed by X-ray diffraction (XRD) using a Malvern PANalytical Empyrean diffractometer with Cu Kα radiation. Continuous scanning with a wavelength of 1.5406 Å at 45 kV and 45 mA was used. The scan speed for the spectrum was 0.5 $min^{-1}$ with a $2\theta$ range of 5–80° at room temperature ($T \approx 21.4$ °C). The lattice constants of the specimen were evaluated by using HighScore Plus V4.9 software. The DSI measurements were performed at room temperature by using a Hystrion Triboindenter (TI-950) with a standard Berkovich tip with a half angle of $\theta = 65.27°$. The constant load holding method[25] was applied to observe the time-dependent plastic deformation by measuring the penetration depth of the indenter, while a constant load is applied on the material's surface for a fixed holding time. Single-crystal $Bi_2Se_3$ samples were cleaved with a surgical blade and a holder[26] in the air atmosphere ($T \approx 21.4$ °C) alongside the (0001) plane. The creep properties of single-crystal $Bi_2Se_3$ were measured using different holding loads, $P$ of 1000, 2000, 3000, 4000, and 5000 μN, respectively. The reliability of all test results was verified by making five independent measurements. An average value was calculated, and the error bars shown in this study represent the standard deviation obtained. The indentation process was completed in four steps, as illustrated in **Figure 1**: loading (at a constant loading rate for 15 s); first holding at the maximum load (600 s); first unloading (15 s); second holding at the %10 of the maximum load (100 s); final unloading (30 s). The second holding step was performed to avoid thermal drift, which can affect the displacements under constant loadings as the measurement area gets smaller.[27]

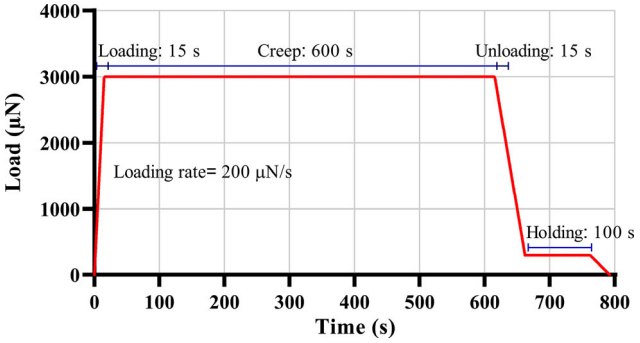


**Figure 1.** Indentation loading profile used for measuring the creep displacement.

Moreover, five different loading times, namely 5 s (1000 μN $s^{-1}$), 15 s (333.33 μN $s^{-1}$), 30 s (166.67 μN $s^{-1}$), 60 s (83.33 μN $s^{-1}$), and 90 s (55.55 μN $s^{-1}$), were applied to the sample under a constant maximum load of 5000 μN to analyze the influence of the strain rate on the creep displacement (i.e., SRS).

## 3. Results and Discussion

### 3.1. X-Ray Diffraction Analysis

The XRD plot shown in **Figure 2** confirmed the single-crystal nature of the manufactured $Bi_2Se_3$ samples, which shows a hexagonal rhombohedral lattice structure belonging to $R\bar{3}m$ space group. The lattice parameters of the $Bi_2Se_3$ single crystal determined by using HighScore Plus V4.9 software are $a = 4.13$ Å, $b = 4.13$ Å, and $c = 28.6$ Å. The XRD plot presenting major sharp (003), (006), (0015), (0018), (0021) peaks and minor (015), (110) peaks indicates that the $Bi_2Se_3$ single crystal is mainly grown along the $c$-axis.

### 3.2. Influence of the Holding Load and Strain Rate Sensitivity

**Figure 3** shows the load versus penetration depth curves obtained using a maximum holding load of 1000, 2000, 3000, 4000, and 5000 μN, respectively. Plastic deformation and residual indentation imprint were observed even at the smallest applied load, which indicates the high ductility of single-crystal $Bi_2Se_3$. Residual imprints of each holding load can be seen in **Figure 4**. As expected, the projected area is increased as the maximum load increased. Small pop-ins (sudden displacement increase in the load–penetration depth curves[28]) were observed during the loading stage and became more obvious as the applied load increased. However, considering the extremely small entity of these pop-ins, and the absence of material damaging on the surface (as shown by the optimal micrographs of Figure 4, the observed pop-ins can be attributed to surface irregularities or experimental noise, rather than nucleation of dislocations of crack initiation. A similar phenomenon has also been observed in the creep experiments of other flexible electronic materials, such as GaAn,[29] $Ni_3Al$,[30] and AZ31 Mg.[31]

The creep displacement–time and strain rate–time curves under varying holding loads are shown in **Figure 5**, which shows data only for the 600 s holding period for all the five different loading profiles of Figure 3. The creep displacement–holding time curves can be evaluated in two distinct phases. The initial creep or transient phase where the creep displacement increases rapidly to a maximum value and then the steady-state creep where the creep displacement hardly deviates and becomes almost linear with the increasing time. It is obviously seen from the figures that the creep displacement initially increases and then tends to stabilize during steady-state creep.[32] For a Berkovich indenter tip, the strain rate $\dot{\varepsilon}$ can be calculated by the following equation:[33]

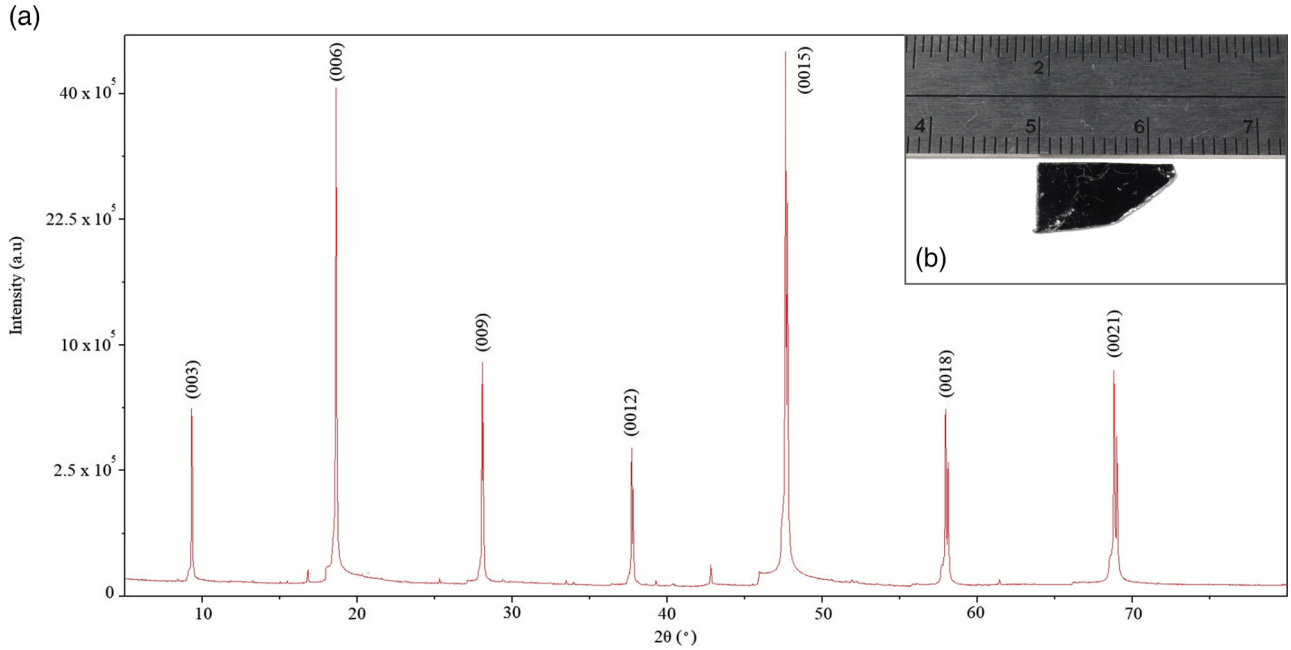


**Figure 2.** a) XRD peaks of single-crystal $Bi_2Se_3$ and b) cleaved surface of as-grown $Bi_2Se_3$ crystal.

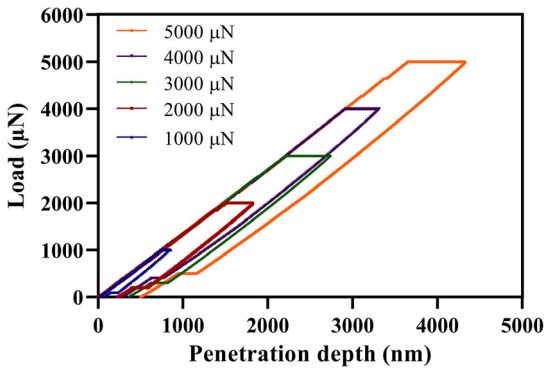


**Figure 3.** Load–penetration depth of single-crystal $Bi_2Se_3$ under different loading profiles.

$$\dot{\varepsilon} = \frac{1}{h_c}\frac{dh_c}{dt} \tag{1}$$

where $h_c$ is the contact penetration depth (i.e., plastic displacement) and $t$ is the holding time. The contact penetration depth $h_c$ can be calculated as $h_c = h - \alpha \times P/S$,[34] where $h$ is the real-time indentation depth, $\alpha$ is an empirical constant equal to 0.72 for a Berkovich tip,[35] $P$ is the applied load, and $S$ is the contact stiffness (i.e., the slope of the unloading portion in the load–penetration depth curve). The real-time indentation depth can be fitted using the following empirical formula ($R^2 > 0.99$):[30]

$$h = h_o + a(t - t_o)^b + kt \tag{2}$$

where $t$ is the time, $h_o$ and $t_o$ are the displacement and time values at the beginning of the load holding stage, and $a$, $b$, and $k$ are fitting parameters. Using Equation (1) and (2), the strain rate$\dot{\varepsilon}$ can be obtained as follows:

$$\dot{\varepsilon} = \frac{a \cdot b \cdot (t - t_o)^{(b-1)} + k}{h_c} \tag{3}$$

As the applied load remains the same during the holding period, as time increases, the strain rate becomes almost constant during the steady-state creep phase. The SRS can be obtained from the slope of the double logarithmic strain rate $\dot{\varepsilon}$ versus hardness $H$ plot during the holding period as follows:

$$m = \frac{\partial \ln(H)}{\partial \ln(\dot{\varepsilon})} \tag{4}$$

where $m$ is the SRS parameter, and the hardness $H$ is defined as

$$H = \frac{P}{A_c} \tag{5}$$

where $A_c$ is the contact area (that increases with increasing values of the applied load by causing a decrease of hardness) calculated as $A_c = \beta \times h_c^2$, where $\beta$ is a geometrical constant equal to 24.3 for a Berkovich tip.[36]

Figure 5 shows the typical two-stage creep displacement–time curves,[37] characterized by an initial stage where the creep displacement (contact depth) rapidly increases over time, and a second steady-state stage where the creep displacement tends to stabilize to a constant value. It is worth noting that the third creep stage related to creep failure[38] is not observed as the tested material did not show any creep damage after 600 s. As expected, larger creep displacements were observed for larger holding loads, as shown in the plots of Figure 5. The plots of Figure 5 show also a good fitting between experimental data and

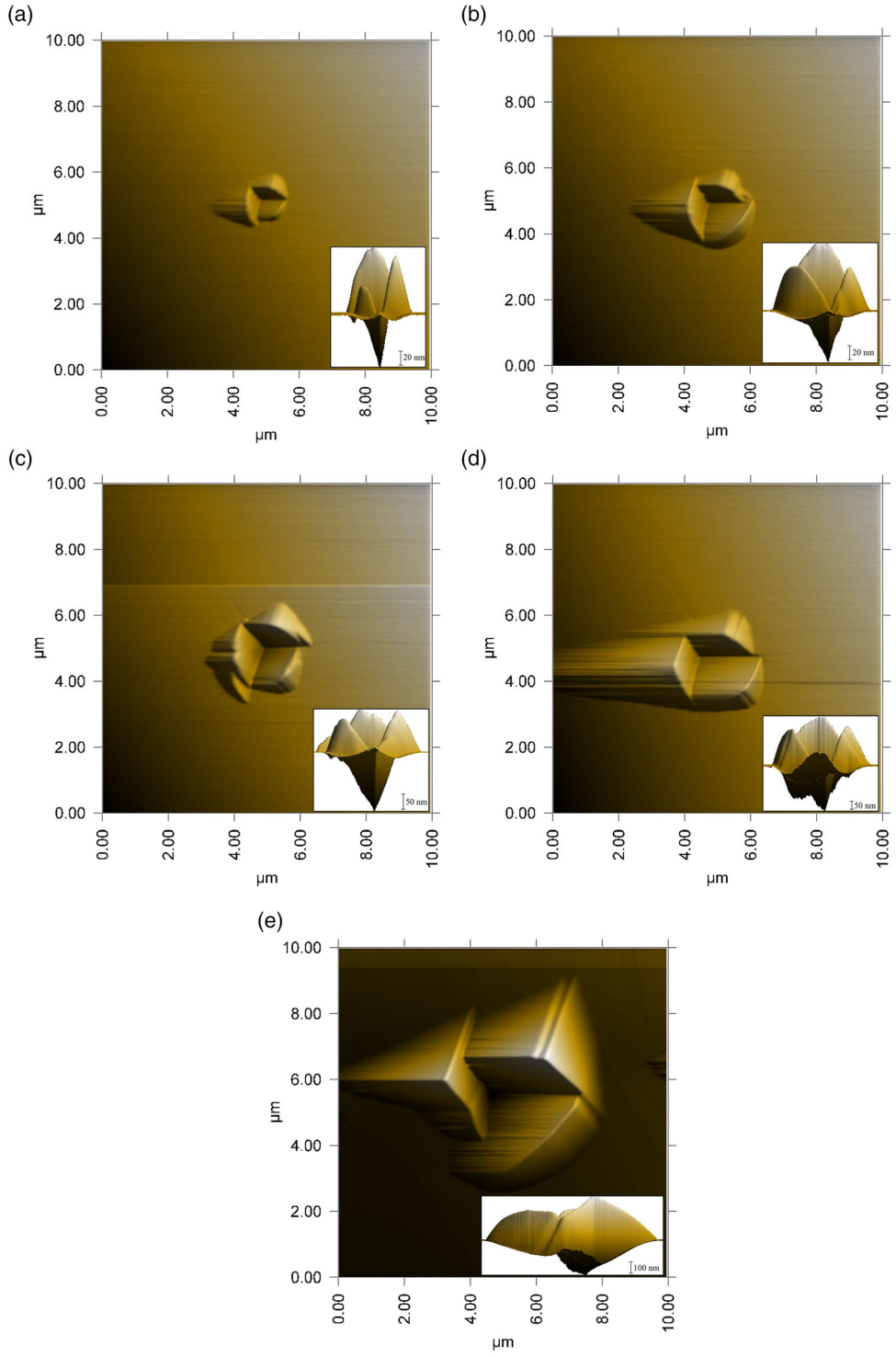


**Figure 4.** Residual imprints of nanoindentation experiments under a maximum holding load of a) 1000 μN, b) 2000 μN, c) 3000 μN, d) 4000 μN, and e) 5000 μN. Insets present the side views of the imprints.

Equation (2) (fitting parameters are shown in tables). A correlation coefficient $R^2 > 0.9$ has been obtained for all curves.

Strain rates were also plotted in the same plots (dashed blue curves). For each holding load, it is observed that the creep strain rate declines rapidly at the beginning of the holding period and becomes constant.

The SRS values of single-crystal $Bi_2Se_3$ were calculated for each maximum holding load using Equation (4). **Figure 6**a shows

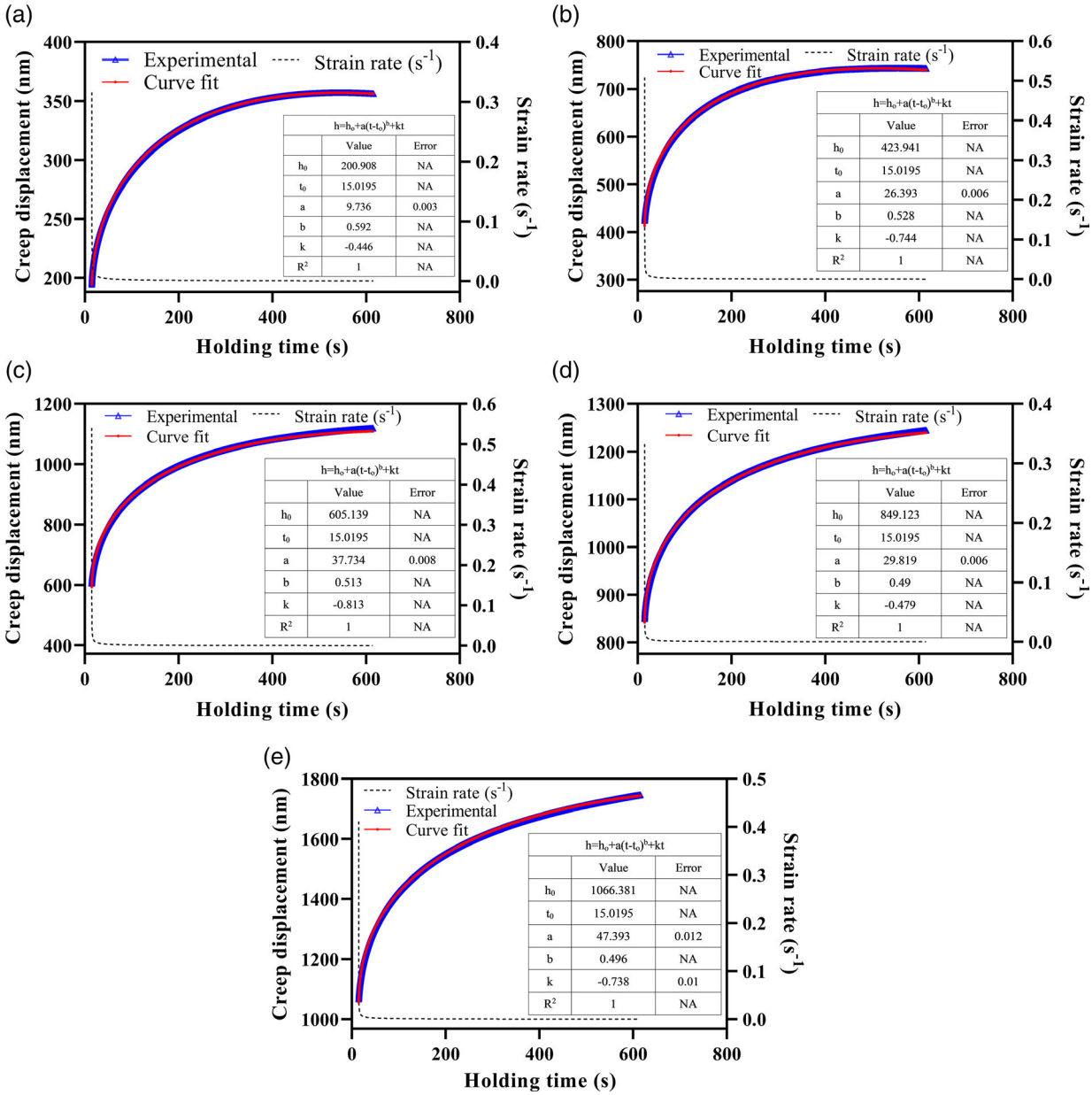


**Figure 5.** Experimental and fitted curves of creep displacement and strain rate versus holding time, for single-crystal $Bi_2Se_3$ at a maximum holding load of a) 1000 μN, b) 2000 μN, c) 3000 μN, d) 4000 μN, and e) 5000 μN.

the SRS parameter $m$, calculated from the slope of the $\log(H)$ versus $\log(\dot{\varepsilon})$ curve, corresponding to a maximum holding load of 1000 μN, while Figure 6b shows SRS values calculated for different values of holding loads. As can be seen from Figure 6b, m decreases from 0.301 to 0.240 with increasing values of holding loads from 1000 to 5000 μN. A sudden drop of $m$ with increasing values of holding loads from 3000 to 4000 μN is noteworthy. The reason for this step change presumably results from inevitable rapid oxidation generated on the surface of $Bi_2Se_3$ after cleavage. SRS is strongly dependent on hardness as described in Equation (6). The hard oxide layer makes it difficult to penetrate the surface and when it is passed, the hardness values and therefore the SRS values are greatly reduced. The decrease of $m$ with increasing holding loads was also observed in other electronic materials, such as Cu[39] and $LiTaO_3$,[38] and indicates that SRS is strongly dependent on indentation penetration size. This phenomenon can be explained from different perspectives. First, the projected area increases as the indenter penetrates the material and this results in stress reduction when a constant load is applied during creep tests. As stress is the driving force for material deformation, such a reduction should decrease the displacement rate until the stress becomes too low to push the tip further into the sample.[40] Thus, the measured value of the SRS should decrease due to its

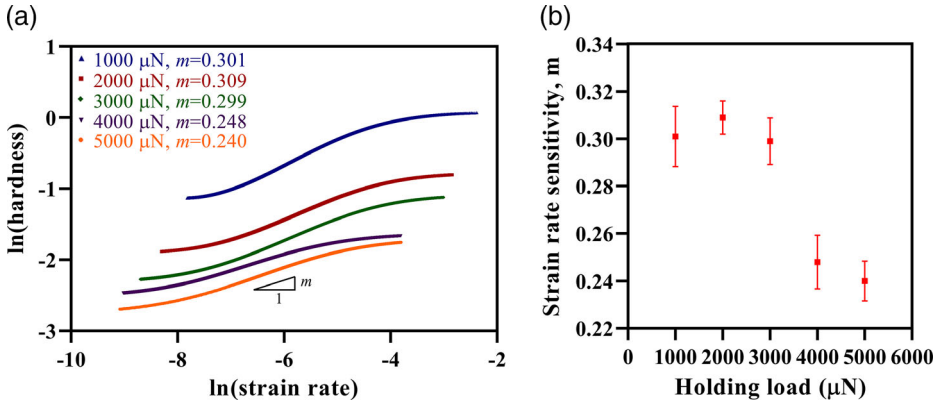


**Figure 6.** a) SRS of single-crystal $Bi_2Se_3$ with constant loading rate under 1000 μN holding load. b) SRS values with standard deviations calculated for different values of holding loads.

inherently reduced deformation as the applied holding load increases. Second, lower loads create lower displacement rates (see Figure 3), which directly affects the hardness considering that $H = P/A$ and the contact area is calculated from maximum displacement ($h_c$), $A = \beta \times h^2$, which tends to be lower at lower holding loads (see Figure 5). According to Equation (5), as the strain rate values during holding at the steady-state creep stage linearized and became almost constant, decreasing hardness values with the reduced displacement activity leads to a reduction in $m$ values between 1000 and 5000 μN.

Moreover, we can affirm that a dislocation-dominated creep behavior has been observed for the tested $Bi_2Se_3$ single crystal, as the creep stress exponent $n$ (i.e., the reciprocal of $m$) varies between 3.69 and 4.081 and then lies in the dislocation-dominated creep range $3 \leq n \leq 6$.[41]

### 3.3. Activation Volume

The activation volume, defined as the volume required to onset the plastic deformation, can be calculated using the following equation:[31,39,42]

$$v^* = Mk_bT\left(\frac{\partial \ln(\dot{\varepsilon})}{\partial(H)}\right) \quad (6)$$

Here, $M$ is the Taylor factor, $k_b$ is the Boltzmann constant, and $T$ is the material temperature. Combining Equation (4) and (6), we can obtain the following simplified equation:

$$v^* = \frac{Mk_bT}{mH} \quad (7)$$

By considering $M = \sqrt{3}$,[43] $k_b = 1.38 \times 10^{-23}$ J K$^{-1}$, and $T = 297.45$ K (i.e., room temperature of 24.3 °C) and using data in Figure 6b, the activation volume $v^*$ can be calculated for different values of holding loads, and results are shown in **Table 1**.

It can be seen from Table 1 that $v^*$ increases from 0.978 b$^3$ to 6.834 b$^3$ for increasing values of the holding load from 1000 to 5000 μN, respectively, where $b$ is the Burgers vector of dislocation, equal to 0.4 for $Bi_2Se_3$.[44] It is noticeable that the activation volume values at 3000 and 4000 μN are very close. This can result from the deformation mechanism at the atomic level. From the micromechanics aspect of view, different deformation mechanisms usually involve specific activation volumes, and $v^*$ between 1 b$^3$ and 10 b$^3$ are associated with dislocation nucleation.[45] The dislocation loops would incubate and grow from the lattice defects, and may ease the onset of plastic deformation.[46] Therefore, defects in the lattice structure at certain regions where 3000 and 4000 uN creep loads are applied can trigger the plastic deformation onset and equalize the $v^*$'s. The overall increase is due to the decrease of $H$ and $m$ for increasing values of holding load $P$ (see Equation (7)). The measured values of the activation volume $v^*$ are very close to those obtained for Cu,[39] by confirming the high ductility of $Bi_2Se_3$ single crystal. According to the results, one can conclude that the large variation of activation volume accounts for the unsteady creep behavior in single-crystal $Bi_2Se_3$ TI.

**Table 1.** The values of activation volume, $v^*$ of single-crystal $Bi_2Se_3$ at various holding loads.

| Holding load [μN] | $v^*$ [b$^3$] |
|---|---|
| 1000 | 0.978 ± 0.098 |
| 2000 | 3.093 ± 0.198 |
| 3000 | 4.681 ± 0.337 |
| 4000 | 4.731 ± 0.512 |
| 5000 | 6.834 ± 0.691 |

### 3.4. Loading Rate Effect

Considering the time-dependent behavior of creep properties, indentation tests have also been performed at different values of loading rate to observe the influence on the creep displacement. **Figure 7**a shows the load–penetration depth curves referred to a maximum holding load of 5000 μN where five different loading rates have been used, namely 5 s (1000 μN s$^{-1}$), 15 s (333.33 μN s$^{-1}$), 30 s (166.67 μN s$^{-1}$), 60 s (83.33 μN s$^{-1}$), and 90 s (55.55 μN s$^{-1}$), while Figure 7b shows the creep displacement obtained during the 600 s holding time for different

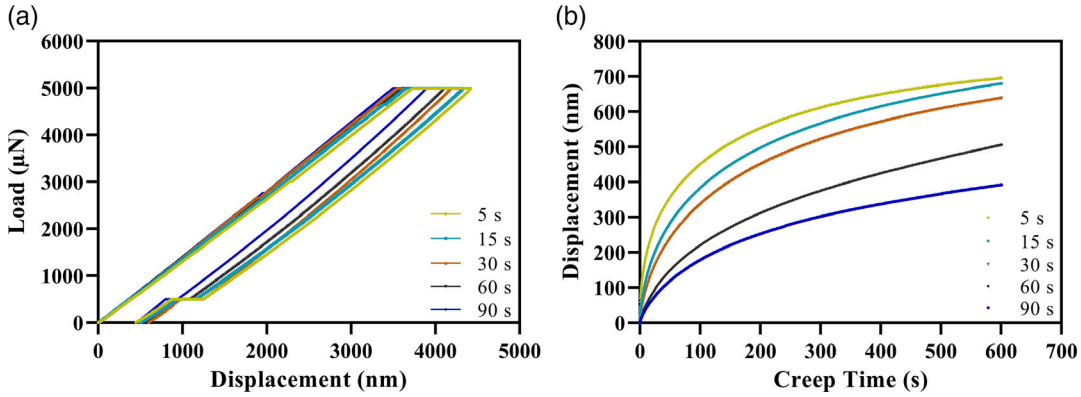


**Figure 7.** a) Load–penetration depth and b) creep displacement–time curves of single-crystal $Bi_2Se_3$ at five different loading times for a maximum holding load of 5000 μN.

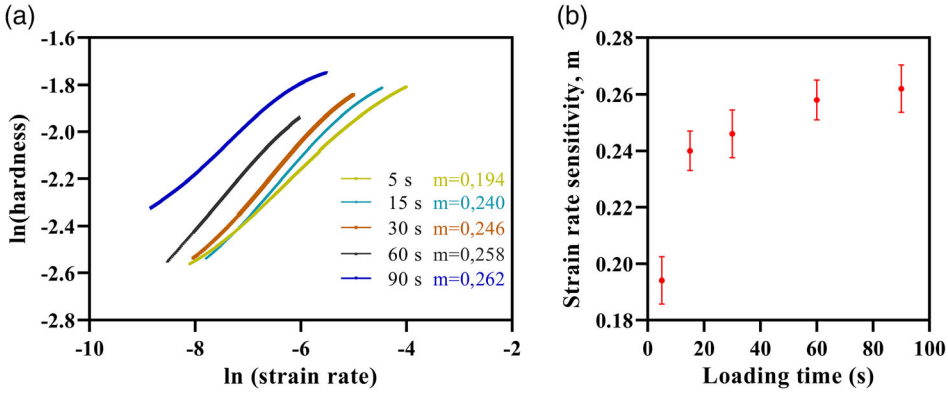


**Figure 8.** a) SRS of single-crystal $Bi_2Se_3$ with different loading times and b) SRS relation to loading time at 5000 μN with standard deviations.

loading rates. It is obvious from the plots of Figure 7a,b that as the loading becomes faster, the creep displacement becomes larger. This is related to the higher energy state, which develops at higher loading rates, that facilitates a larger viscoplastic deformation.[47,48]

**Figure 8**a,b shows the *m* values obtained for different loading rates. From the figures, it is clearly seen that SRS increases significantly with increasing loading time from 5 to 15 s (this is because load holding times lower than 20 s are likely to be less affected by thermal-drift induced errors[40]), while a slight increase is observed from 15 to 90 s.

The increasing values of *m* with increasing loading rates were reported for other materials. Ma[48] et al. observed that the SRS of annealed CoCrFeCuNi HEA film increased with increasing loading rate compared to the as-deposited film because the annealing process caused stabilization at the inner structure of the material. In other studies, Sharma et al.[49] and Ma et al.[50] reported a positive correlation between SRS and loading rate while investigating the nanoindentation creep behavior of HgCdTe and Ni, respectively. However, there are other studies which observed an opposite behavior. Mahmudi et al.[41] reported an increase of *n* values (and then a decrease of *m* values) with increasing loading rate and declared that *n* does not depend on the loading conditions.

We observed that for the tested $Be_2Se_3$ sample, the SRS does not strongly depend on the loading rate (*m* values are in fact almost stable between 15 and 90 s). This is related to the single-crystal nature of the tested material. The loading rate strongly influences the SRS in polycrystal materials, where the dislocation nucleation is influenced by grain boundaries.[39] The absence of grain boundaries in our single-crystal material makes the loading rate influence less strong.

However, research on the relationship between the SRS and the loading rate is limited to date. This behavior should be carefully taken into consideration and further research is required to shed more light on this mechanism.

## 4. Conclusion

In this work, single-crystal $Bi_2Se_3$ TI was grown using the Bridgman–Stockbarger method. Nanoindentation creep properties of single-crystal $Bi_2Se_3$, such as creep deformation, SRS, and activation volume, were investigated at various loading rates and holding loads to shed some light on the scale- and time-dependent behavior of the tested material.

Experimental results revealed that the creep displacement of the material increased with increasing values of the maximum

holding load from 1000 to 5000 μN. Accordingly, the activation volume increased, and the SRS decreased with the increase of the holding load. A scale effect related to the load applied and then the area of the material tested by indentation was then observed. The creep displacement during the holding stage increased with increasing values of loading rate due to the higher energy state, which develops at higher loading rates, that facilitates a larger viscoplastic deformation. A positive correlation between loading time and SRS was observed and attributed to the single-crystal nature of the $Bi_2Se_3$ sample.

Finally, the results obtained also confirmed a high ductility of the tested material and dislocation-dominated creep behavior.

The proposed results provide useful information on the scale- and time-dependent mechanical properties of the single-crystal $Bi_2Se_3$ TI, by paving the way for the design of novel and cutting-edge $Bi_2Se_3$-based devices.

## Acknowledgements

This work was partly supported by the Scientific Research Projects Unit (BAP) of Zonguldak Bulent Ecevit University (Project code no: 2019-77654622-01). U.U. would like to thank TUBITAK 2214-A – International Doctoral Research Fellowship Programme for supporting his research at the University of Iowa.

## Conflict of Interest

The authors declare no conflict of interest.

## Data Availability Statement

The data that support the findings of this study are available on request from the corresponding author. The data are not publicly available due to privacy or ethical restrictions.

## Keywords

activation volume, bismuth selenide, creep, single crystal, strain rate, strain rate sensitivity

Received: September 15, 2021
Revised: November 26, 2021
Published online: January 19, 2022

[1] C. L. Kane, E. J. Mele, *Phys. Rev. Lett.* **2005**, *95*, 226801.
[2] L. Fu, C. L. Kane, E. J. Mele, *Phys. Rev. Lett.* **2007**, *98*, 106803.
[3] C. Nayak, S. H. Simon, A. Stern, M. Freedman, S. Das Sarma, *Rev. Mod. Phys.* **2008**, *80*, 1083.
[4] S. Manna, P. Wei, Y. Xie, K. T. Law, P. A. Lee, J. S. Moodera, *Proc. Natl. Acad. Sci. USA* **2020**, *117*, 8775.
[5] A. R. Mellnik, J. S. Lee, A. Richardella, J. L. Grab, P. J. Mintun, M. H. Fischer, A. Vaezi, A. Manchon, E.-A. Kim, N. Samarth, D. C. Ralph, *Nature* **2014**, *511*, 449.
[6] M. Z. Hasan, C. L. Kane, *Rev. Mod. Phys.* **2010**, *82*, 3045.
[7] T. Chudoba, N. M. Jennett, *J. Phys. D* **2008**, *41*, 215407.
[8] N. P. Butch, K. Kirshenbaum, P. Syers, A. B. Shuskov, G. S. Jenkins, H. D. Drew, J. Paglione, *Phys. Rev. B: Condens. Matter Mater. Phys.* **2010**, *81*, 241301(R).
[9] M. Woodhouse, A. Goodrich, R. Margolis, T. L. James, M. Lokanc, R. Eggert, *IEEE J. Photovoltaics* **2013**, *3*, 833.
[10] X. Luo, M. B. Sullivan, S. Y. Quek, *Phys. Rev. B: Condens. Matter Mater. Phys.* **2012**, *86*, 184111.
[11] A. Sharma, B. Bhattacharyya, A. K. Srivastava, T. D. Senguttuvan, S. Husale, *Sci. Rep.* **2016**, *6*, 19138.
[12] H.-D. Lai, S.-R. Jian, L. T. C. Tuyen, P. H. Le, C.-W. Luo, J.-Y. Juang, *Micromachines* **2018**, *9*, 518.
[13] S. Gupta, N. Vijayan, A. Krishna, K. Thukral, *J. Appl. Crystallogr.* **2015**, *48*, 533.
[14] H. Yan, C. Vajner, M. Kuhlman, L. Guo, L. Li, P. T. Aroujo, H.-T. Wang, *Appl. Phys. Lett.* **2016**, *109*, 032103.
[15] H. Zhu, C. A. Richter, E. Zhao, J. E. Bonevich, A. K. William, H.-J. Jang, H. Yuan, H. Li, A. Arab, O. Kirillov, J. E. Maslar, D. E. Ioannou, Q. Li, *Sci. Rep.* **2013**, *3*, 1757.
[16] C. Yue, S. Jiang, H. Zhu, L. Chen, Q. Sun, D. W. Zhang, *Electronics* **2018**, *7*, 225.
[17] Y. Hu, M. Tong, X. Cheng, J. Zhang, H. Hao, J. You, X. Zheng, T. Jiang, *ACS Photonics* **2020**, *8*, 771.
[18] A. C. Fisher-Cripps, *Mater. Sci. Eng. A* **2004**, *385*, 74.
[19] P. Z. Bažant, *Mathematical Modeling of Creep and Shrinkage of Concrete*, Wiley, Evanston, IL, USA, **1988**.
[20] R. S. Ginder, W. D. Nix, G. M. Pharr, *J. Mech. Phys. Solids* **2018**, *112*, 552.
[21] E. Broitman, *Tribol. Lett.* **2017**, *65*, 23.
[22] V. V. Atuchin, V. A. Golyashov, K. A. Kokh, I. V. Korolkov, A. S. Kozhukhov, V. N. Kruchinin, S. V. Makarenko, L. D. Pokrovsky, I. P. Prosvirin, K. N. Romanyuk, O. E. Tereshchenko, *Cryst. Growth Des.* **2011**, *11*, 5507.
[23] A. Politano, V. M. Silkin, I. A. Nechaev, M. S. Vitiello, L. Viti, Z. S. Aliev, M. B. Babanly, G. Chiarello, P. M. Echenique, E. V. Chulkov, *Phys. Rev. Lett.* **2015**, *115*, 216802.
[24] U. Uzun, M. Yetmez, N. Akıncı, *Micro Nano Lett.* **2021**, *16*, 203.
[25] R. Goodall, T. W. Clyne, *Acta Mater.* **2006**, *54*, 5489.
[26] C. Lamuta, A. Cupolillo, A. Politano, Z. S. Aliev, M. B. Babanly, E. V. Chulkov, L. Pagnotta, *Nano Res.* **2016**, *9*, 1032.
[27] V. Maier, B. Merle, M. Göken, K. Durst, *J. Mater. Res.* **2013**, *28*, 1177.
[28] F. Pöhl, *Sci. Rep.* **2019**, *9*, 15350.
[29] S. A. S. Asif, J. B. Pethica, *Philos. Mag. A* **1997**, *76*, 1105.
[30] H. Li, A. H. W. Ngan, *J. Mater. Res.* **2004**, *19*, 513.
[31] J. Hu, W. Zhang, G. Peng, T. Zhang, Y. Zhang, *Mater. Sci. Eng. A* **2018**, *725*, 522.
[32] J. Dean, A. Bradbury, G. Aldrich-Smith, T. W. Clyne, *Mech. Mater.* **2013** *65*, 124.
[33] B. N. Lucas, W. C. Oliver, *Metall. Mater. Trans. A* **1999**, *30*, 601.
[34] W. C. Oliver, G. M. Pharr, *J. Mater. Res.* **2004**, *19*, 3.
[35] H. Bei, E. P. George, J. L. Hay, G. M. Pharr, *Phys. Rev. Lett.* **2005**, *95*, 045501.
[36] W. C. Oliver, G. M. Pharr, *J. Mater. Res.* **1992**, *7*, 1564.
[37] G. Feng, A. H. W. Ngan, *J. Mater. Res.* **2002**, *17*, 660.
[38] Y. Ma, X. Huang, Y. Song, W. Hang, T. Zhang, *Materials* **2019**, *12*, 1683.
[39] W. Sun, Y. Jiang, G. Sun, J. Hu, T. Zhou, Z. Jiang, J. Lian, *Mater. Sci. Eng. A* **2019**, *751*, 35.
[40] D. Peykov, E. Martin, R. R. Chromik, R. Gauvin, M. Trudeau, *J. Mater. Sci.* **2012**, *47*, 7189.
[41] R. Mahmudi, R. Roumina, B. Raeisinia, *Mater. Sci. Eng. A* **2004**, *382*, 15.
[42] S. Mishra, V. K. Beura, A. Singh, M. Yadava, N. Nayan, *Mater. Sci. Eng. A* **2018**, *729*, 102.
[43] Y. M. Wang, A. V. Hamza, E. Ma, *Acta Mater.* **2006**, *54*, 2715.

[44] A. Zhuang, J. J. Li, Y.-C. Wang, X. Wen, Y. Lin, B. Xiang, X. Wang, J. Zeng, *Angew. Chem. Int. Ed.* **2014**, *53*, 6425.
[45] M. A. Monclús, J. M. Molina-Aldareguia, in *Handbook of Mechanics of Materials* (Eds. C.-H. Hsueh, S. Schmauder, C.-S. Chen, K. K. Chawla, N. Chawla, W. Chen, Y. Kagawa), Springer, Singapore **2019**, pp. 2219–2247.
[46] D. Wang, J. Tan, C. J. Li, X. M. Qin, S. F. Guo, *J. Alloys Compd.* **2021**, *885*, 161038.
[47] P. Gong, J. Jin, L. Deng, S. Wang, J. Gu, K. Yao, X. Wang, *Mater. Sci. Eng. A* **2017**, *688*, 174.
[48] Y. Ma, G. J. Peng, D. H. Wen, T. H. Zhang, *Mater. Sci. Eng. A* **2015**, *621*, 111.
[49] H. K. Sharma, R. Prasad, R. S. Saxena, A. Gokhale, R. K. Sharma, *Def. Sci. J.* **2020**, *70*, 493.
[50] Z. Ma, S. Long, Y. Pan, Y. Zhou, *J. Mater. Sci.* **2008**, *43*, 5952.